Journal of
Composites Science

MDPI

Article

Synthesis of Hematite Nanodiscs from Natural Laterites and Investigating Their Adsorption Capability of Removing Ni^{2+} and Cd^{2+} Ions from Aqueous Solutions

B. P. N. Gunawardhana [1], C. A. Gunathilake [2,*], K. E. D. Y. T. Dayananda [1], D. M. S. N. Dissanayake [1,3], M. M. M. G. P. G. Mantilaka [1,3], C. S. Kalpage [2], R. M. L. D. Rathnayake [4], R. M. G. Rajapakse [1,5], A. S. Manchanda [6], Thusitha N. B. Etampawala [7], B. G. N. D. Weerasekara [8], P. N. K. Fernando [9] and Rohan S. Dassanayake [10]

1 Postgraduate Institute of Science (PGIS), University of Peradeniya, Peradeniya 22400, Sri Lanka; nishh902@gmail.com (B.P.N.G.); taniya9922@gmail.com (K.E.D.Y.T.D.); nilsandun@hotmail.com (D.M.S.N.D.); mantilaka@gmail.com (M.M.M.G.P.G.M.); rmgr@pdn.ac.lk (R.M.G.R.)
2 Department of Chemical & Process Engineering, Faculty of Engineering, University of Peradeniya, Peradeniya 22400, Sri Lanka; csk@eng.pdn.ac.lk
3 Sri Lanka Institute of Nanotechnology (SLINTEC), Mahenwatta, Pitipana, Homagama 10206, Sri Lanka
4 Department of Civil Engineering, Faculty of Engineering, University of Peradeniya, Peradeniya 22400, Sri Lanka; englashi@gmail.com
5 Department of Chemistry, Faculty of Science, University of Peradeniya, Peradeniya 22400, Sri Lanka
6 Department of Chemistry, California State University, Stanislaus, One University Circle, Turlock, CA 95382, USA; amanpb19@gmail.com
7 Department of Polymer Science, Faculty of Applied Sciences, University of Sri Jayewardenepura, Nugegoda 10100, Sri Lanka; tetampa@sjp.ac.lk
8 Department of Nano Science Technology, Faculty of Technology, Wayamba University of Sri Lanka, Kuliyapitiya 60200, Sri Lanka; nuwandweerasekara@gmail.com
9 Department of Chemistry, Faculty of Graduate Studies, University of Kelaniya, Kelaniya 11300, Sri Lanka; nimedhafernando@gmail.com
10 Department of Biosystems Technology, Faculty of Technology, University of Sri Jayewardenepura, Gangodawila, Nugegoda 10100, Sri Lanka; rdassanayake@sjp.ac.lk
* Correspondence: chamilag@pdn.ac.lk; Tel.: +94-718-311-117

Received: 23 March 2020; Accepted: 14 May 2020; Published: 20 May 2020

Abstract: In this work, disc-like hematite (Fe_2O_3) nanoparticles were prepared using a readily available inexpensive earth material, ferruginous laterite, via a low-cost synthesis route. Prepared hematite nanoparticles were characterized using X-Ray diffraction (XRD), inductively coupled plasma mass spectroscopy (ICP-MS), particle size analyzer (PSA), Fourier transform infrared (FT-IR) spectroscopy, scanning electron microscopy (SEM), and nitrogen adsorption-desorption analyzer. The performance of hematite nanoparticles was evaluated as a heavy metal ion adsorbent. Batch adsorption experiments were conducted to study the adsorption behaviour of Ni^{2+} and Cd^{2+} ions as a function of the amount of adsorbent, contact time, and pH. Adsorption data fitted to the linearized Langmuir and Freundlich kinetic models were compared and discussed. The correlation coefficient (R^2) was used to determine the best fit kinetic model. Our data fitted the Langmuir kinetic model well and the highest adsorption efficiencies were found to be 62.5 mg/g for Ni^{2+} and 200 mg/g for Cd^{2+}, respectively. Due to high surface area, pore volume with active sites, and sorption capabilities, hematite nanoparticles can be used as efficient and economical nano-adsorbents for the removal of Ni^{2+} and Cd^{2+} ions from industrial wastewater.

Keywords: hematite nanoparticles; adsorption; water treatment; heavy metals

1. Introduction

Heavy metals are metallic elements or metalloids that have high atomic weights in the range of 63.5 and 200.6 g/mol and specific gravities greater than 5.0. Most heavy metals are toxic even at low concentrations (<0.1 ppm) and non-biodegradable inside living organisms and hence bio-accumulate through food chains [1–5]. They can cause severe health issues, such as irreversible kidneys, brain, and nervous system damage, and consequently leading to cancer [2,6–12]. Heavy metals are also extremely harmful to flora, fauna, and all anthropogenic life. Cadmium (Cd^{2+}) and nickel (Ni^{2+}) are two of the most commonly found heavy metal ions in industrial effluents of textile, plastics, paints, furniture processing, construction, electronics, petroleum smelting, alloy, and battery industries. However, the treatment of Cd^{2+} and Ni^{2+} ions from industrial effluents is extremely costly and much money is spent on removing these heavy metals around the globe [1–5].

Generally, an industrial effluent purification system should be efficient, simple, environmentally-friendly, and economical. However, currently available purification systems for removing heavy metals from industrial effluents are expensive and they use chemicals that in turn release harmful substances into water streams during the treatment processes [3–7]. To solve this issue, adsorption techniques have been introduced [1,5–7,13–25]. Among many sorbents reported, activated carbon is widely studied for removing heavy metals from wastewater streams [14,25]. However, the use of activated carbon produced from various sources in industrial effluent purifications is limited, due to their high production costs [6,7,13]. Additionally, the weak physical interaction between activated carbon and heavy metals has made it less effective [6,13].

Several low-cost materials including kaolinite [19], montmorillonite [19], burnt brick particles [20], peat [21,22], maize cob [23], and rice husks [24] have been recently introduced for the removal of heavy metals. The use of nanoparticles as adsorbents for removing heavy metals has gained significant attention due to their unique chemical and physical properties as compared to bulk materials [4,5,8,15–18,25]. However, the synthesis of many nanoparticle-based adsorbents requires advanced techniques and expensive raw materials [1,8,13,16,17]. It is, therefore, of interest to synthesize nanomaterials via simple methods utilizing low-cost raw materials.

Laterites are readily available, extensively distributed, and cheap natural earth materials that can be potentially used as raw materials for synthesizing inorganic nanomaterials. In contrast to many disputes about the definition of laterites, laterites can be simply explained as highly weathered natural clay materials with high concentrations of iron or aluminum oxides [26,27]. Table 1 shows the physical and chemical properties of natural laterites. Laterites are also comprised of large amounts of quartz and kaolinite. There is also evidence that the early African tribes used laterites as a source of iron [7]. Furthermore, most metal-based industries around the world use laterites as a source of producing other elements such as aluminum, manganese, nickel, titanium, and chromium [28]. Laterites are widely utilized for construction and dwellings applications. Over the last few years, the main application of laterites as bricks has been plummeting with the introduction of cheap building materials such as cement blocks and metal sheets. Although there is a high potential of laterites to be used in synthesizing value-added iron-based nanomaterials, limited work has been conducted so far. Commonly studied iron-based nanomaterials include magnetite (Fe_3O_4) [29], goethite(α-FeOOH) [30], and hematite(Fe_2O_3) [31–33]. Among those, hematite nanoparticles have been investigated for a range of applications, including adsorption [18,34–37], water splitting [38,39], photochemical [40,41], catalytic [40,42], and electrochemical [43,44] processes.

In the current work, we focus on the facile and economically feasible synthesis of disc-like hematite nanoparticles using naturally abundant laterites. Here it is also reported the use of hematite nanoparticles for their effective removal of Ni^{2+} and Cd^{2+} via the adsorption process.

Table 1. Physical and chemical properties of natural laterites [26,27].

Chemical Composition	Values (%)	Engineering and Physical Properties	Values
SiO_2	21.55	pH	5.35
Al_2O_3	24.31	Specific gravity	2.69
Fe_2O_3	29.40	External surface area (m^2 g^{-1})	42.0
Na_2O	0.07	Maximum dry density (mg m^{-3})	1.31
K_2O	0.11	Optimum moisture content (%)	34.0
P_2O_5	16.71	Unconfined compressive strength (kPa)	270.0
SO_3	3.98	-	-
CO_2	3.65	-	-

2. Materials and Methods

2.1. Materials

Iron-rich laterites were obtained from the Homagama area of Sri Lanka. Sodium hydroxide (NaOH) pellets (98% (*w*/*w*) purity) and hydrochloric acid (HCl, 36.5% (*v*/*v*) assay) were purchased from Euclid suppliers, Cleveland, OH, USA. Sodium dodecyl sulfate (SDS, 85% (*w*/*w*) assay) was purchased from Labachemia suppliers, Milano, Italy. Cadmium chloride ($CdCl_2$) and nickel chloride ($NiCl_2$) were obtained from Hopkins & Williams Ltd., Manselton, UK; BDH laboratory reagents, Muscat, Oman.

2.2. Synthesis of Hematite Nanoparticles

The powdered and dried iron-rich laterites were acid digested at 109 °C with 12 M HCl until the solution became yellow (laterite: acid ratio (*w*/*v*%) = 1:3). Then the solution was cooled and filtered. The filtrate was stirred vigorously with 10 mL of SDS on a stirrer for 15 min. A 3.5 M NaOH (filtrate: NaOH ratio (*w*/*v*%) = 1:4) solution was added dropwise into the above mixture with continuous stirring until a reddish-brown precipitate was formed. The mixture was centrifuged at 4500 rpm and further stirred for 1 h. The reddish-brown precipitate was collected and heated at 110 °C for 4 h. Finally, the dark red solid product was calcined at 800 °C for 2 h. Note that the particle size of the hematite nanoparticles is governed by the NaOH concentration. Hematite nanoparticles synthesized were used for Ni^{2+} and Cd^{2+} adsorption studies.

2.3. Characterization

The particle size of prepared hematite nanomaterials was analyzed using a particle size analyzer (ZEN3600). A Rigaku Ultima IV X-ray diffractometer (XRD) equipped with radiation source Cu Kα and a single curved crystal graphite monochromator (λ = 1.54056 nm) was used in XRD analysis of the synthesized nanoparticles. An Agilent 7900 inductively coupled plasma mass spectroscopy (ICP-MS) was used for the elemental analysis of the adsorbent. Fourier Transform Infra-Red (FT-IR) spectra of the nanoparticles were obtained using a Bruker Vertex 80 FT-IR spectrometer with Hyperion 1000 ATR microscopy accessory. A Hitachi SU6600 scanning electron microscope (SEM) was used to observe the morphology of the prepared hematite nanoparticles.

2.4. Nitrogen Adsorption Studies

Nitrogen adsorption isotherms of synthesized hematite nanoparticles were measured at −196 °C on an ASAP 2010 volumetric analyzer (Micromeritics, Inc., Norcross, GA, USA). Prior to the adsorption measurements, all samples were outgassed under vacuum at 110 °C for 2 h.

2.5. Calculations of Surface Properties

The single-point pore volume (V_{sp}) was estimated from the amount adsorbed at a relative pressure (p/p°) of ~ 0.98. The pore size distributions (PSD) were calculated using adsorption branches of nitrogen adsorption-desorption isotherms by the improved KJS method calibrated for cylindrical pores [40].

The pore width (W_{max}) was obtained at the maximum of the PSD curve. The Brunauer-Emmett-Teller specific surface areas (S_{BET}) were calculated from the N_2 adsorption isotherms in the relative pressure range of 0.05–0.20 using a cross-sectional area of 0.162 nm^2 per nitrogen molecule.

2.6. Adsorption Studies

2.6.1. Preparation of Stock Metal Ion Solutions

1000 ppm nickel (Ni^{2+}) and cadmium (Cd^{2+}) stock solutions were prepared, respectively, by dissolving the analytical grade nickel chloride ($NiCl_2$) and cadmium chloride ($CdCl_2$) in deionized water.

2.6.2. pH Optimization

100 ppm Ni^{2+} and Cd^{2+} solutions were prepared from their respective stock solutions. Solutions of different pH values (3–10) were prepared either by adding a 3.5 M NaOH or a 5 M HCl solution. For each solution, 0.300 g of prepared hematite nanoparticles was added and stirred for 120 min. These treated solutions were centrifuged at 4000 rpm and the supernatant was filtered off. Filtrates were diluted and used to measure the equilibrium concentrations.

2.6.3. Mass Optimization

A series of 100 mL of 100 ppm Ni^{2+} and Cd^{2+} solutions were prepared from their respective stock solutions with pH adjusted to pH 6 for Cd^{2+} and pH 6.5 for Ni^{2+} by adding appropriate amounts of 3.5 M NaOH and 5 M HCl solutions. These solutions were stirred with 0.10, 0.20, 0.26, 0.28, 0.30, 0.32, 0.34, 0.36, and 0.40 g of prepared hematite nanoparticles for 120 min on a stirrer. These treated solutions were centrifuged at 4000 rpm and supernatants were filtered off. The filtrates were diluted and used to measure the equilibrium concentrations.

2.6.4. Kinetic Study

A series of 100 mL of 100 ppm Ni^{2+} (pH 6.5) and Cd^{2+} (pH 6) solutions were prepared from their respective stock solutions by adding appropriate amounts of 3.5 M NaOH or 5 M HCl solution. Prepared Cd^{2+} and Ni^{2+} solutions were stirred with 0.32 and 0.30 g of prepared hematite nanoparticles, respectively, on a stirrer for 240 min. 0.5 mL of each solution was pipetted out from the stirring solution at time intervals of 0, 30, 60, 90, 120, 150, 180, 210, and 240 min. These treated solutions were centrifuged at 4000 rpm and supernatants were filtered. Finally, the filtered solutions were diluted and used to determine the equilibrium concentrations.

2.6.5. Equilibrium Studies

A solution series (100 ppm, 200 ppm, 300 ppm, 400 ppm) of Ni^{2+} and Cd^{2+} solutions were prepared from their respective stock solutions. The Cd^{2+} solutions were adjusted to pH 6 and Ni^{2+} solutions were adjusted to pH 6.5. Prepared Cd^{2+} solutions and Ni^{2+} solutions were stirred with 0.32 and 0.30 g of hematite nanoparticles, respectively, on a stirrer for 120 min. These treated solutions were centrifuged at 4000 rpm and supernatants were filtered. The filtered solutions were diluted and measured for equilibrium concentrations using an Agilent 7900 Inductively Coupled Plasma Mass Spectroscopy (ICP-MS). All experiments were carried out at room temperature and atmospheric pressure (1 atm). The results were evaluated using the Langmuir and Freundlich adsorption isotherm models.

2.6.6. Adsorption Isotherms

$$RE\% = \left(\frac{C_0 - C_e}{C_0}\right) \times 100\% \quad (1)$$

The equilibrium concentration of each solution represents the average of three independent measurements. Removal efficiencies (RE %) were calculated using Equation (1), where C_0 (mg L^{-1}) is the initial adsorbate concentration, and C_e (mg L^{-1}) is the equilibrium adsorbate concentration [41].

$$q_e = \frac{(C_0 - C_e)V}{m} \quad (2)$$

The adsorption capacities (q_e) of Ni^{2+} and Cd^{2+} adsorbed onto hematite nanoparticles were calculated using Equation (2), where C_0 (mg L^{-1}) is the initial adsorbate concentration, C_e (mg L^{-1}) is the equilibrium adsorbate concentration, V(L) is the volume of solution, and m is the mass (g) of adsorbent [41].

$$\left(\frac{C_e}{q_e}\right) = \left(\frac{1}{q_m}\right) \times C_e + \left(\frac{1}{q_m K_L}\right) \quad (3)$$

Adsorption isotherms were plotted using the calculated adsorption capacities and equilibrium concentrations. Equation (3) shows the linearized form of the Langmuir monolayer adsorption Isotherm, where C_e is the equilibrium concentration of adsorbate in solution (mg L^{-1}), q_e is the equilibrium adsorption capacity of adsorbent (mg g^{-1}), q_m is the highest adsorption capacity of adsorbent (mg g^{-1}), and K_L is the Langmuir constant [41].

$$\ln q_e = \left(\frac{1}{n}\right) \ln C_e + \ln K_F \quad (4)$$

Similarly, Freundlich Isotherm which describes the multi-layer adsorption can be linearized as shown in Equation (4), where C_e is the equilibrium concentration of adsorbate (mg L^{-1}), q_e is the equilibrium adsorption capacity of adsorbent (mg g^{-1}), and K_F and n are the Freundlich constants [41].

$$\ln\left(q_e - q_t\right) = \ln\left(q_e\right) - k_1 t \quad (5)$$

Adsorption kinetics can be used to optimize the time consumption of an adsorption process. The pseudo-first-order kinetic model suggests that the kinetics of the adsorption process depends on the adsorbate concentration rather than the adsorbent concentration. Equation (5) shows the pseudo-first-order kinetic model, where q_e is the equilibrium adsorption capacity of adsorbent (mg g^{-1}), q_t is the adsorption capacity of adsorbent at time t (mg g^{-1}), t is the time elapsed (min), and k_1 is the rate constant (g mg^{-1} min^{-1}) [45,46].

$$\frac{t}{q_t} = \left(\frac{1}{k_2 q_e^2}\right) + \frac{t}{q_e} \quad (6)$$

Equation (6) shows the Pseudo-second order kinetic model, where q_e is the equilibrium adsorption capacity of adsorbent (mg g^{-1}), q_t is the adsorption capacity of adsorbent at time t (mg g^{-1}), t is the time elapsed (min), and k_2 is the rate constant (g mg^{-1} min^{-1}). This model suggests that the kinetics of the adsorption process depends on the adsorbent concentration rather than the adsorbate concentration. Generally, it considers the adsorption site concentration [45,46]. All adsorption measurements were conducted in triplicates. Equilibrium concentrations (C_e) and adsorption capacities (q_e) used in the two kinetic models are the average values of at least three independent measurements at each concentration.

3. Results

3.1. Synthesis of Hematite Nanoparticles

In the synthesis process, acid digestion of laterite involves the digestion of the major constituents; Al_2O_3 and Fe_2O_3, into their chloride forms. Equations (7) and (8) show the reactions involved in the acid digestion of laterites:

$$Fe_2O_{3(s)} + 6HCl_{(aq)} \rightarrow 2FeCl_{3(aq)} + 3H_2O_{(l)} \quad (7)$$

$$Al_2O_{3(s)} + 6HCl_{(aq)} \rightarrow 2AlCl_{3(aq)} + 3H_2O_{(l)} \quad (8)$$

After acid digestion, the solution is filtered off to remove acid-insoluble constituents such as SiO_2. The resulting solution was mixed with SDS and stirred continuously with the dropwise addition of NaOH. Here the SDS acts as a stabilizer to prevent the highly active nanoparticle agglomeration, responsible for particle size adjustments and works as a template. The excess NaOH in the solution precipitates as $Fe(OH)_3$ and $AlCl_3$ reacts with NaOH to form $NaAlO_2$ as shown in Equations (9)–(11):

$$FeCl_{3(aq)} + 3NaOH_{(aq)} \rightarrow Fe(OH)_{3(s)} + 3NaCl_{(aq)} \quad (9)$$

$$AlCl_{3(aq)} + 3NaOH_{(aq)} \rightarrow Al(OH)_{3(s)} + 3NaCl_{(aq)} \quad (10)$$

$$Al(OH)_{3(s)} + NaOH_{(aq)} \rightarrow NaAlO_{2(aq)} + 2H_2O_{(l)} \quad (11)$$

SDS is partially and $NaAlO_2$ is fully removed during the washing and centrifugation steps of $Fe(OH)_3$. However, calcination at 800 °C ensures the complete removal of SDS. Note that the optimal concentration of 3.5 M NaOH was added to acid digested mixture to completely convert $Al(OH)_3$ to $NaAlO_2$. Therefore, no residual $Al(OH)_3$ was present in the final mixture.

3.2. Characterization of Synthesized Hematite Nanoparticles

Results obtained from the particle size analyzer (PSA) confirmed that the average particle size of hematite particles is 37.5 nm. Figure 1a shows the PSA profile of the monodispersed hematite sample with an average diameter of 37.5 nm. Note that the average particle size of the hematite nanoparticles is governed by the concentration of NaOH added to the acid digested laterite solution.

Figure 1b shows the XRD diffractogram of the hematite nanoparticles. The XRD peaks, which attribute to (012), (104), (110), (113), (024), (116), (122) and (018) crystalline planes, are in agreement with the literature values reported for pure α-Fe_2O_3 hematite nanoparticles (See Figure 1b) [47,48]. ICP-MS (Table 2) and XRD (Figure 1c) data further confirm the formation of hematite nanoparticles (α-Fe_2O_3) with a mass percentage of 97.17%. The absence of XRD peaks for $NaAlO_2$ or $Al(OH)_3$ confirm the complete removal of $NaAlO_2$ during the filtration and washing steps [47,48].

Table 2. ICP-MS analysis of hematite nanoparticles.

	Element	Composition/%
(1)	Fe	97.17
(2)	Al	0.32
(3)	Na	0.05
(4)	V	0.02

FTIR spectrum of hematite nanoparticle is shown in Figure 1c. The vibration band observed at 588.54 cm^{-1} is attributed to the stretching vibrations of Fe-O bonds of hematite (Fe_2O_3). The bands at 464.23 cm^{-1} and 419.68 cm^{-1} correspond to the formation of α-Fe_2O_3. Lack of the vibration band at 708 cm^{-1} confirms the absence of hydrated iron (Fe-OH). This further indicates the conversion of ferric hydroxide ($Fe(OH)_3$) to hematite (Fe_2O_3). No vibration peaks were observed for SDS confirming

the complete removal of SDS during the calcination. The absence of vibration peaks for $NaAlO_2$ or $Al(OH)_3$ further confirms their complete removal during filtration and washing steps. Other major peaks at 3506.58, 3380.61, 3048.04, 1652.26 cm^{-1} are assigned to physically adsorbed moisture (H_2O vapor) and the vibration band at 1487.34 cm^{-1} represents carbon dioxide adsorbed onto the highly reactive surface of the nanomaterials [49,50].

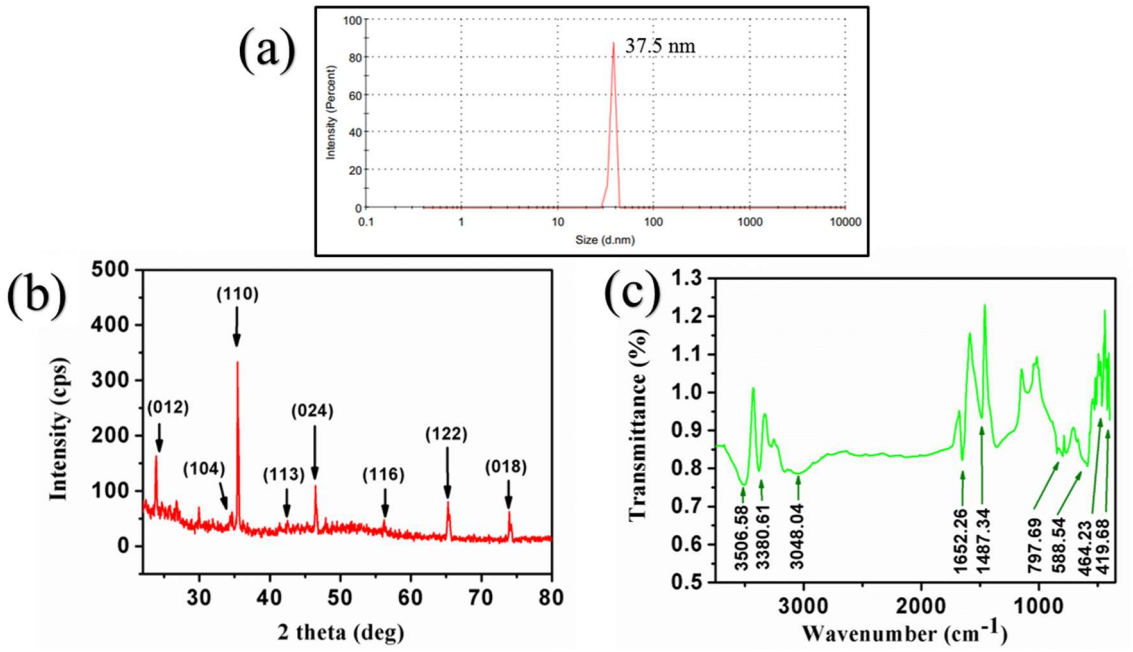

Figure 1. (**a**) Particle size distribution (**b**) XRD and (**c**) FTIR pattern of the hematite particles synthesized.

Figure 2 displays the digital photograph of synthesized hematite nanoparticles which is reddish brown in colour. Figure 3 shows the SEM images of hematite nanoparticles at four different magnifications. At low magnifications, hematite nanoparticles exhibit a spherical shape (see Figure 3a,b). As can be seen from Figure 3c,d, hematite nanoparticles show disc-like morphology at higher magnifications. Interestingly, hematite nanoparticles with different morphologies, including pseudocubic, pseudoellipsoidal, octahedral, rhombohedral, and plate-like hexagonal have also been reported previously [51–53].

Figure 2. Digital photograph of hematite nanoparticles.

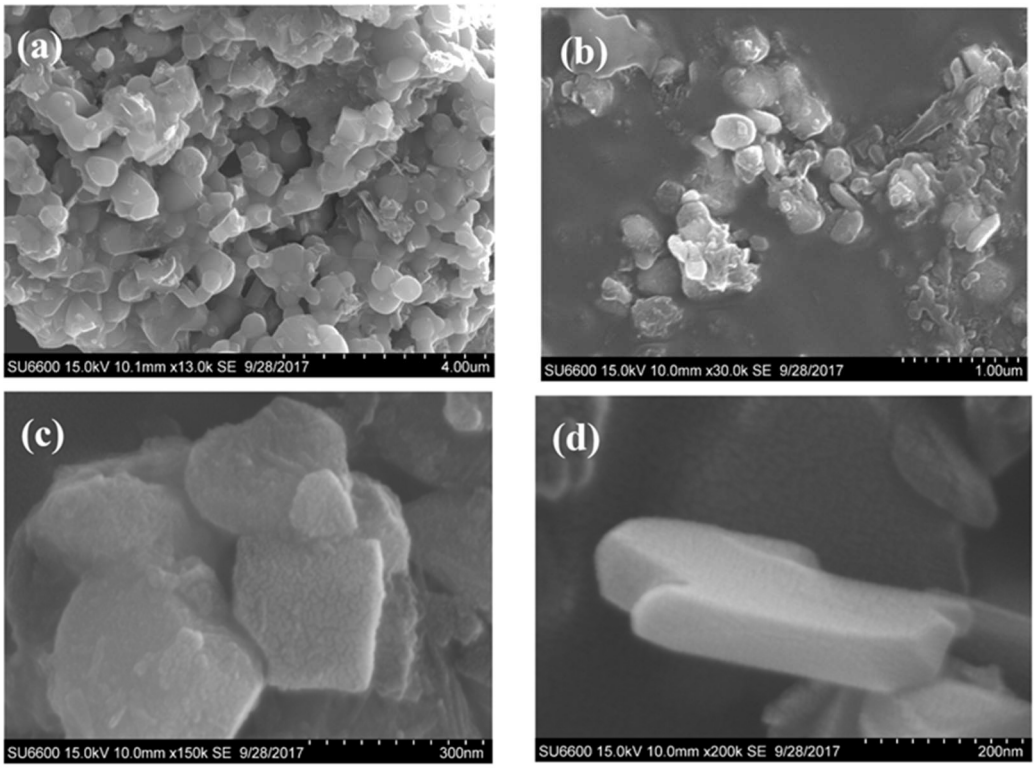

Figure 3. SEM images of hematite nanoparticles powder at (**a**) 4 μm, (**b**) 1 μm, (**c**) 300 nm, and (**d**) 200 nm magnifications, respectively.

3.3. Nitrogen Adsorption Studies

Nitrogen adsorption isotherms were measured at −196 °C on an ASAP 2010 volumetric analyzer for hematite nanoparticles with an average diameter of 37.5 nm. Figure 4 displays the nitrogen adsorption-desorption isotherms measured at −196 °C for synthesized hematite nanoparticles. Structural parameters calculated based on the nitrogen sorption data are shown in Table 3. Nitrogen adsorption isotherm of hematite nanoparticles shows a type IV isotherm with a H1 type hysteresis loop characteristic for mesoporous materials. The sample exhibits a capillary condensation-evaporation step in the relative pressure range of ~0.80–0.98. This type of isotherms with the H1 hysteresis loop represents characteristic cylindrical pores.

Table 3. Adsorption parameters for the Hematite nanoparticle (Hematite NP) samples studied.

Content	Particle Diameter (nm)	MLC (cc STP/g)	V_{sp} (cc/g)	V_{mi} (cc/g)	S_{BET} (m^2/g)	W_{max} nm	V_t (cc/g)
Hematite NP	37.5	2.53	0.02	<0.01	11.03	2.5/20.2	0.04

The total pore volume and specific surface area recorded for nanoparticles are ~0.04 cm^3/g and 11.03 m^2/g, respectively. However, the calculated micropore volume for the hematite nanoparticles is less than 0.01 cm^3/g. PSD curve for the nanoparticles is shown in Figure 4, right panel. The nanoparticles showed W_{max} at 20.2 nm and 2.5 nm.

Particle Diameter was obtained from particle size analyzer, MLC-Monolayer capacity, V_{sp}-single-point pore volume calculated at the relative pressure of 0.98; V_{mi}—the cumulative pore volume of micropores, (pores below 2 nm) was calculated on the basis of the KJS method; S_{BET}—specific surface area calculated from adsorption data in relative pressure range 0.05–0.20; W_{max}—pore width

calculated at the maximum of PSD, using improved KJS method; V_t—total pore volume calculated by integration of the PSD curve [54,55].

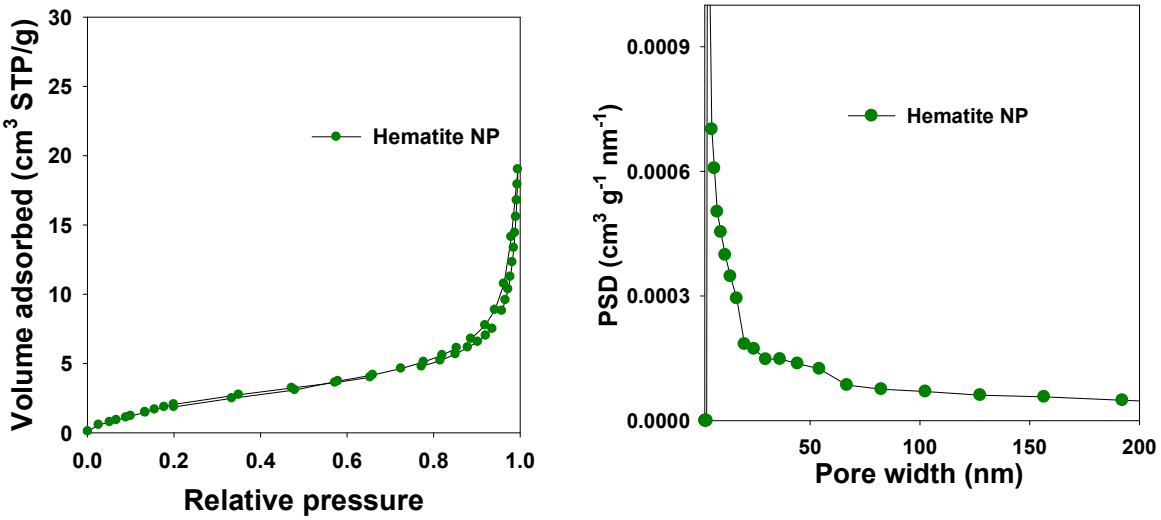

(**a**) (**b**)

Figure 4. N_2 adsorption isotherms (**a**) and their corresponding PSD curve (**b**) for hematite nanoparticle studied.

3.4. Heavy Metal Sorption

The removal efficiency of Ni^{2+} and Cd^{2+} by hematite nanoparticles from aqueous solution was calculated using Equation (1). The removal efficiencies (RE%) of Ni^{2+} and Cd^{2+} by hematite nanoparticles at four different adsorbate concentrations are tabulated in Table 4. As can be seen from Table 4, the highest RE% value of 80.50% and 95.95% was observed at 100 ppm initial concentration for $Ni^{2+}$and Cd^{2+}, respectively. The RE% decreases as the concentration of initial $Ni^{2+}$and Cd^{2+} increases due to the saturation of adsorbent sites available on the adsorbent. Interestingly, Ni^{2+} showed a slightly higher decrement of RE% as compared to Cd^{2+} with increasing concentration.

Table 4. Removal efficiencies (RE %) of hematite nanoparticles at different concentrations of $Ni^{2+}$and Cd^{2+} ions.

Initial Concentration/ppm	RE% of Ni^{2+}	RE% of Cd^{2+}
100	80.50 ± 0.04	95.95 ± 0.08
200	72.41 ± 0.07	94.29 ± 0.08
300	50.58 ± 0.02	92.89 ± 0.05
400	43.93 ± 0.07	91.21 ± 0.02

3.5. Langmuir Adsorption Isotherm Studies

Langmuir constants and maximum adsorption capacities of each ion calculated using the linearized Langmuir adsorption isotherm (see Figure 5) are tabulated in Table 5.

$$R_L = \frac{1}{(1 + (K_L C_0))} \quad (12)$$

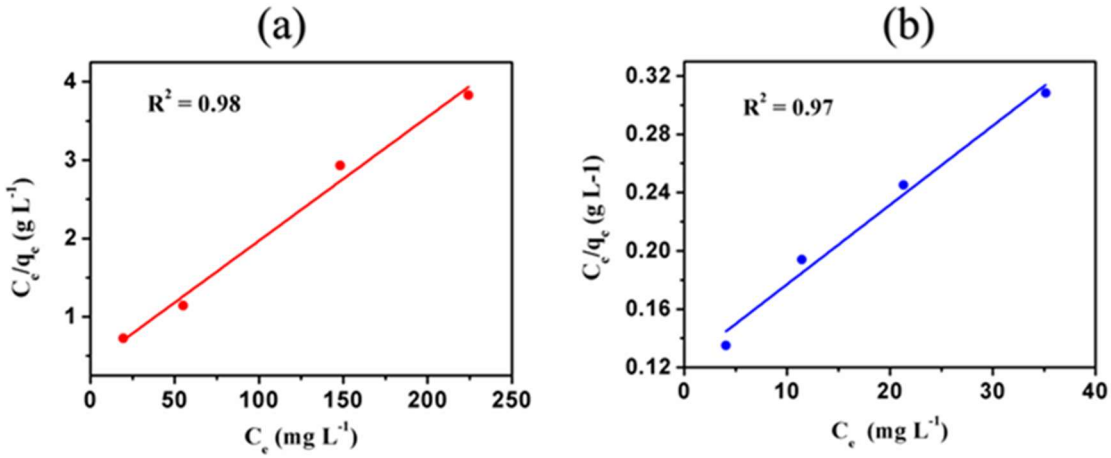

Figure 5. Langmuir isotherms of (**a**) Ni^{2+} and (**b**) Cd^{2+} by hematite nanoparticles.

Table 5. Langmuir adsorption isotherm constants of Ni^{2+} and Cd^{2+} ions adsorbed onto hematite nanoparticle.

Ion	Q_m/mg g^{-1}	K_L/L mg^{-1}	Regression (R^2)
Ni^{2+}	62.50 ± 0.05	$(4.07 \times 10^{-2}) \pm 0.07$	0.98
Cd^{2+}	200.00 ± 0.08	$(4.10 \times 10^{-2}) \pm 0.05$	0.97

The separation factor or equilibrium parameter denoted as R_L of both ions is calculated using Equation (12) and tabulated in Table 6, where K_L is the Langmuir constant (L/mg), and C_0 is the initial concentration of adsorbate (mg/L). The separation factor of both Ni^{2+} and Cd^{2+} lies in the range of 0.058 to 0.197. Since the R_L value of both ions is between 0 and 1, the data follow a monolayer adsorption mechanism [56,57]. Typically, the monolayer adsorption mechanism is a clear indication of the chemisorption of absorbate onto the adsorbent.

Table 6. Separation factors (R_L) at each adsorbate concentration.

C_0 (Ppm)	R_L for Ni^{2+}	R_L for Cd^{2+}
100	0.197	0.196
200	0.109	0.109
300	0.076	0.075
400	0.058	0.058

3.6. Freundlich Adsorption Isotherm

Figure 6 shows the Freundlich isotherms of Cd^{2+} and Ni^{2+} ions adsorbed onto hematite nanoparticles. The Freundlich isotherms were constructed using Equation (4) and the Freundlich constants calculated are tabulated in Table 7.

Table 7. Freundlich adsorption isotherm constants for Ni^{2+} and Cd^{2+} ions adsorbed onto hematite nanoparticles.

Ion	1/n	K_F	Regression (R^2)
Ni^{2+}	0.29 ± 0.04	12.30 ± 0.15	0.80
Cd^{2+}	0.62 ± 0.03	12.93 ± 0.48	0.99

As can be seen from R^2 values in Table 7, the adsorption of Cd^{2+} by hematite nanoparticles fitted comparatively well to the Freundlich model as compared to Ni^{2+}. Moreover, the Freundlich plots show

positive values for Freundlich constants and positive gradients for both Cd^{2+} and Ni^{2+} ions. Therefore, Freundlich isotherms suggest multilayer adsorption of Cd^{2+} and Ni^{2+} ions onto hematite nanoparticles.

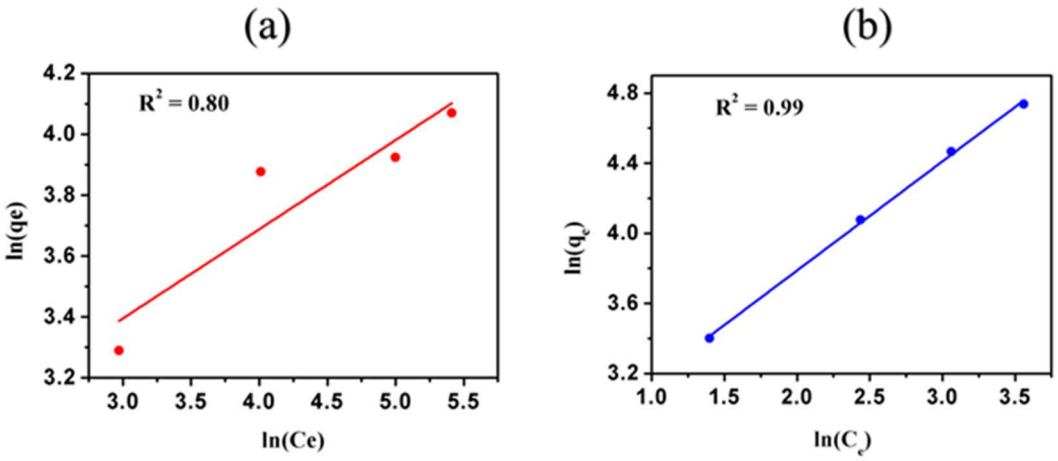

Figure 6. Freundlich isotherms of (**a**) Ni^{2+} and (**b**) Cd^{2+} by hematite nanoparticles.

Cd^{2+} and Ni^{2+} ions show a combination of the monolayer (chemisorption) and partial multilayer adsorption (physisorption). The value of $\left(\frac{1}{n}\right)$ is < 1, which indicates a typical adsorption process where adsorbates show reversible interactions with the adsorbent showing a multilayer adsorption mechanism. This also suggests the possibility of reusing the adsorbent [56,57]. The isotherms in Figures 5 and 6 are plotted from the data collected from batch experiments conducted in a selected range of concentrations of heavy metal ions from 100 to 400 ppm.

Based on the two models applied, the adsorption data of Ni^{2+} ions fitted well to the Langmuir model, whereas the adsorption data of Cd^{2+} followed the Freundlich model. These results reveal that the adsorption of Ni^{2+} by hematite nanoparticles is predominantly via the chemisorption process. This is further proven by the RE% data of Ni^{2+}. The RE% (removal efficiencies) values of Ni^{2+} decrease significantly as the Ni^{2+} concentration increases indicating the complete saturation of the active sites on the adsorbent and hence no further adsorption occurs. On the contrary, the RE% values of Cd^{2+} did not show a significant decrease and remained around 90% as the concentration of Cd^{2+} increases, suggesting the adsorption is via both chemisorption and physisorption processes. Here the adsorption process further continues via physisorption even after the saturation of active sites on the adsorbent is reached.

3.7. pH Optimization

Figures 7 and 8 show the plots of the adsorption capacity and the removal efficiency of the samples at different pH values. The pH values at which the adsorption capacity and removal efficiency reach the highest are selected as the optimum pH value for the adsorption of two ions onto hematite nanoparticles. The optimum pH obtained for Ni^{2+} and Cd^{2+} is pH 6.5 and 6.0, respectively. Data collected at optimum pH values were used in kinetic models.

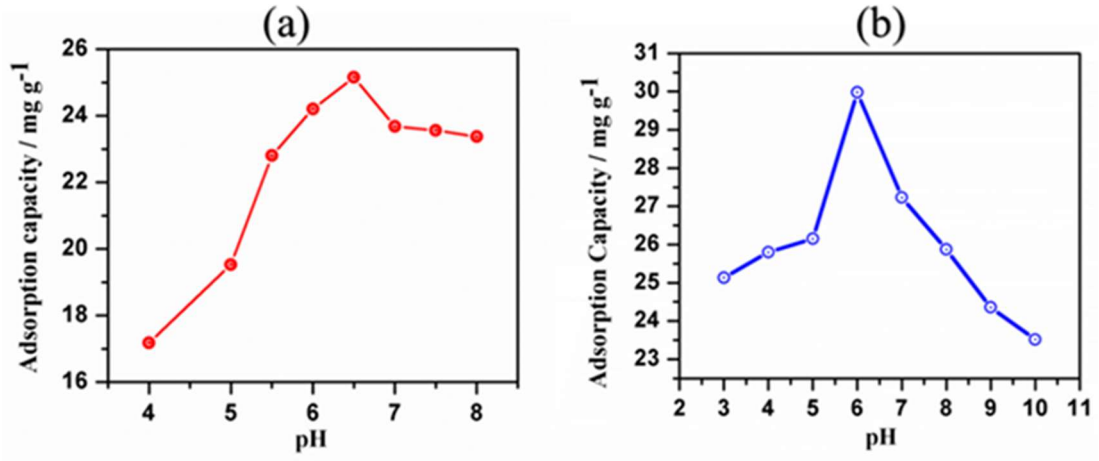

Figure 7. Plot of adsorption capacity of (**a**) Ni^{2+} and (**b**) Cd^{2+} by hematite nanoparticles vs. pH.

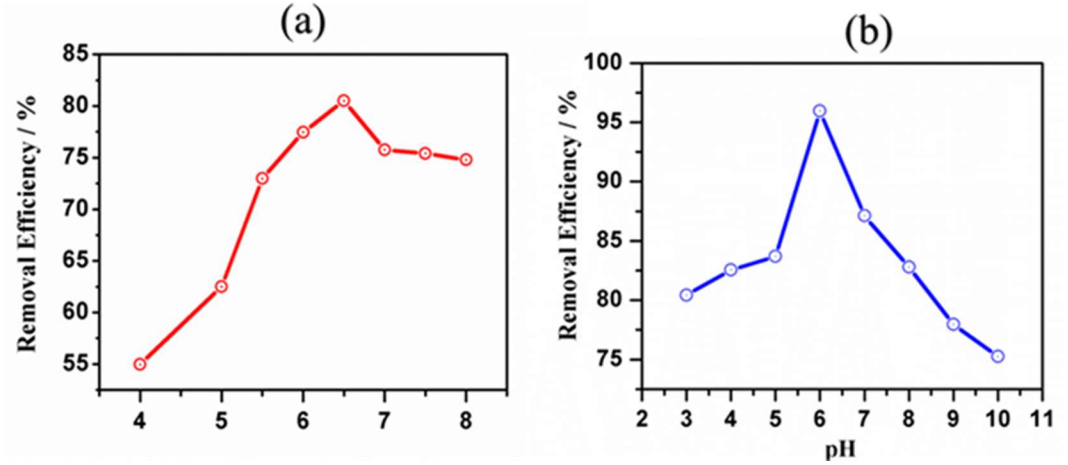

Figure 8. The pH dependency of the removal efficiency (RE%) of (**a**) Ni^{2+} and (**b**) Cd^{2+} ions by hematite nanoparticles.

3.8. Mass Optimization

The amount of adsorbate adsorbed is directly proportional to the adsorption capacity of the nanomaterial. Therefore, the adsorbate removal quantity [initial concentration (C_0)—equilibrium concentration (C_e)] is plotted against a gradient of the adsorbent amount. The optimized amount of adsorbent needed for maximum removal efficiency is obtained from the non-linear regression of the following plots in Figure 9. The optimum amount of adsorbent for Ni^{2+} and Cd^{2+} is 0.30 g and 0.32 g, respectively.

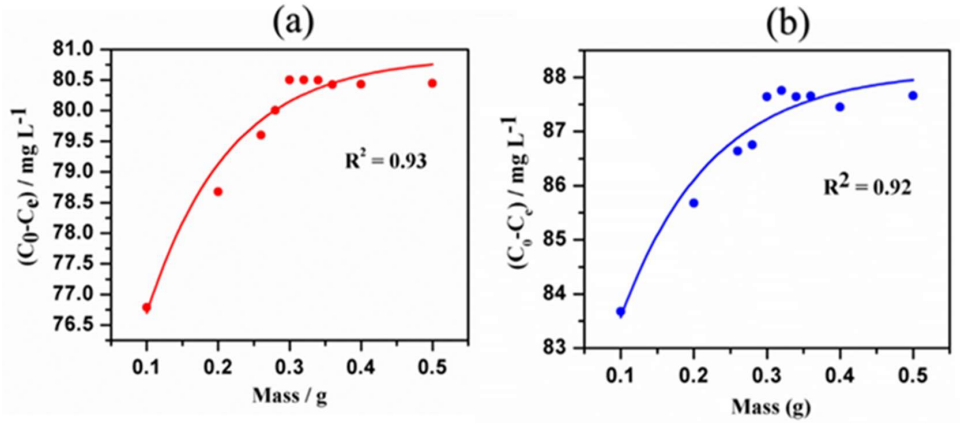

Figure 9. Plot of amount adsorbed of (**a**) Ni^{2+} and (**b**) Cd^{2+} ions by hematite nanoparticles with increasing mass.

3.9. Kinetics Studies

Kinetic studies provide valuable information about the rate of Ni^{2+} and Cd^{2+} uptake by hematite nanomaterials, their reaction pathways, and possible binding mechanisms. The variation of adsorption capacity over time and pseudo-second-order kinetics are plotted in Figures 10 and 11, respectively. Regression data (R^2) of both kinetic models suggest that the data fitted well to the second-order model as compared to the first-order model (data not provided).

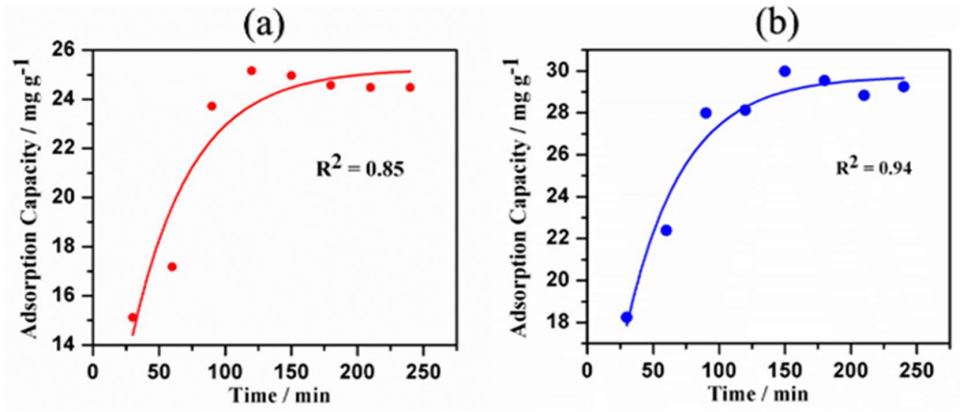

Figure 10. A plot of adsorption capacity of (**a**) Ni^{2+} and (**b**) Cd^{2+} ions adsorbed onto hematite nanoparticles over time.

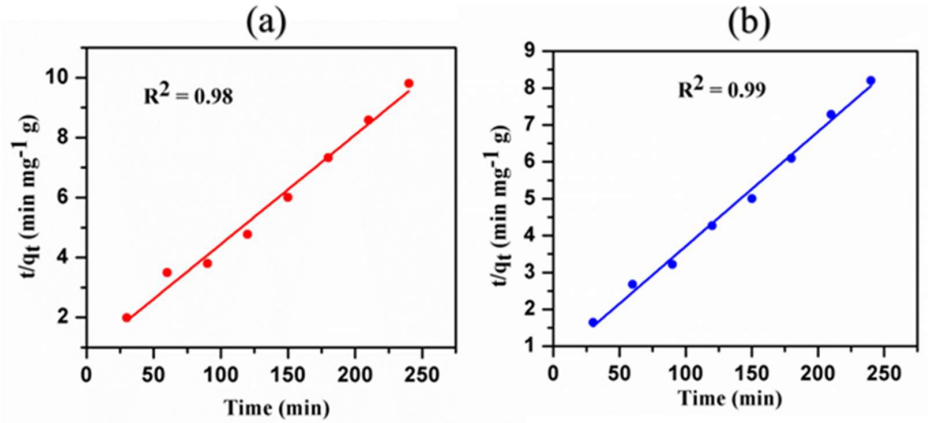

Figure 11. Pseudo-second order model of (**a**) Ni^{2+} and (**b**) Cd^{2+} ions adsorbed onto hematite nanoparticles.

3.10. Adsorption Mechanisms

The study of two adsorption isotherms of Ni^{2+} and Cd^{2+} showed a similar adsorption mechanism [58,59]. As revealed by previous studies, monolayer coverage is explained by the Langmuir isotherm, which describes the chemisorption. During this process, metal ions bind to the specific sites of the absorbent with much stronger interactions, however, the reversible desorption process occurs only under specific conditions such as pH and temperature. The multilayer coverage is explained by the Freundlich model indicating the physisorption where the metal ions bind to the adsorbent with much weaker interactions via Van der Waals forces, hence the reversible desorption process could occur under normal conditions.

The Fe-O functional groups of hematite are responsible for the chemisorption of metal ions. The hematite is made up of two ferric (III) ions in octahedral coordination with three oxide ions in hexagonal close-packing. Each ferric ion and oxide ion in hematite molecule possesses a positive charge of +3 and a negative charge of −2, respectively. Hence, the overall charge of the hematite molecule is zero. The electron density distribution of the molecule suggests that the overall charge of the molecule is not neutral at all the time due to the uneven distribution of electrons in its atomic orbitals. This principle is called the electron density distribution heterogeneity, which explains the physisorption via weak Van der Walls interactions between metal ions and hematite nanoparticles.

In addition, it is reasonable to assume that the chemisorption is through the coordination between O^- or OH^- groups available on hematite nanomaterials with Ni^{2+} and Cd^{2+}. The chemisorption process can be well explained using the Pearson HSAB (hard-soft acid-base) theory. Based on the HSAB concept, hard acids like binding to the hard bases, resulting in strong ionic complexes. Both Ni^{2+} and Cd^{2+} are hard acids, and hence form strong ionic interactions with hard bases such as O^- or OH^-.

The hematite nanoparticles showed monolayer adsorption capacities of 62.5 for Ni^{2+} and 200.00 mg g^{-1} for Cd^{2+}, and multilayer adsorption capacities of 12.30 mg g^{-1} for $Ni^{2+}$and 12.93 mg g^{-1} for Cd^{2+}, respectively, (See Tables 5 and 7). The hematite nanoparticles exhibited strong monolayer chemisorption weak reversible multilayer physisorption with both metal ions. However, data for Cd^{2+} fitted well to both kinetic models with a regression value above 97%. Data for Ni^{2+} did not fit well to the Freundlich model giving a regression value of 80%. This suggests that the physisorption process of Ni^{2+} ions by hematite nanoparticles is less favourable.

3.11. Possible Applications of This Adsorption Process

Thus far, different types of adsorbents have been used for heavy metal removal. However, many of them inherit certain drawbacks such as energy extensive nature, high cost of processing, low efficiencies, and lower adsorption capacities [50]. Nevertheless, the hematite nanomaterials reported in the present study have many promising properties as compared to other adsorbents; they include relatively easy synthesis route, low cost, and less energy requirement. Interestingly, our material also shows higher removal efficiencies and high adsorption capacities of Ni^{2+} and Cd^{2+} comparable to the other adsorbents reported in the literature (see Table 8).

The ability of the prepared hematite nanomaterial to adsorb Ni^{2+} and Cd^{2+} can be mainly used in the remediation process of industrial effluents contaminated with heavy metals. Due to relatively higher adsorption towards heavy metals, this material can also be used in water purification filters.

The ability of the prepared hematite nanomaterial to adsorb Ni^{2+} and Cd^{2+} can be mainly used in the remediation process of industrial effluents contaminated with heavy metals. Due to relatively higher adsorption towards heavy metals, this material can also be used in water purification filters.

Note that it is reasonable to assume the possibility of releasing a negligible amount of hematite nanomaterials to the aqueous solution during the centrifugation and filtration steps of the synthesis. However, the leached-out nanoparticles can be recycled and used for other applications [56,57,64]. Therefore, our synthesis route is environmentally friendly and a green approach. Most importantly, our synthesis procedure is well suited for the preparation of large-scale filters that can be used for the removal of industrial heavy metal waste effluents.

Table 8. Comparison of Cd^{2+} and Ni^{2+} ions adsorbents and their maximum adsorption capacities [14,60–64].

Adsorbent	Heavy Metal Ion	Maximum Adsorption Capacity/mg g^{-1}	References
Activated carbon	Ni(II)	400.0	[14,60–62]
	Cd(II)	178.5	
CNT * modified with hydroxyquinoline	Ni(II)	4.2	[63]
CNT *	Cd(II)	10.9	[64]
Laterite derived-hematite nanoparticles	Ni(II)	62.5	Current study
	Cd(II)	200.0	Current study

* CNT = Carbon Nanotubes.

4. Conclusions

A facile and low-cost method was successfully devised to synthesize hematite nanomaterials from laterites. The sorption ability of hematite nanoparticles for the removal of Ni^{2+} and Cd^{2+} heavy metal ions was also investigated. The highest adsorption capacities of 62.5 mg g^{-1} and 200.00 mg g^{-1} were observed for Ni^{2+} and Cd^{2+}, respectively. The hematite nanoparticles derived from laterites show the potential to remove heavy metals from industrial effluents. Furthermore, this study also paves the way for the preparation of value-added filter materials from naturally abundant iron-rich laterite ores.

Author Contributions: Writing & Editing, B.P.N.G., C.A.G., K.E.D.Y.T.D., D.M.S.N.D., M.M.M.G.P.G.M., C.S.K., R.M.L.D.R., R.M.G.R., A.S.M., T.N.B.E., B.G.N.D.W., P.N.K.F.; Review & Editing, C.A.G. and R.S.D. All authors have read and agreed to the published version of the manuscript.

Funding: This research was funded by the National Research Council (NRC) of Sri Lanka under grant number [16-123]. Sri Lanka Institute of Nanotechnology covered some of the cost of analysis.

Acknowledgments: Authors would like to acknowledge the support given by the staff at the Physical Research Laboratory, Peradeniya University, Peradeniya, Sri Lanka, and the NRC of Sri Lanka for their financial assistance.

Conflicts of Interest: The authors declare no conflict of interest.

References

1. Shukla, A.K.; Alam, J.; Alhoshan, M.; Dass, L.A.; Ali, F.A.A.; Muthumareeswaran, M.R.; Mishra, U.; Ansari, M.A. Removal of heavy metal ions using a carboxylated graphene oxide-incorporated polyphenlsulfone nanofiltration membrane. *Environ. Sci. Water Res. Technol.* **2018**, *4*, 297–305. [CrossRef]
2. Salam, O.E.A.; Reiad, N.A.; ElShafei, M.M. A study of the removal characteristics of heavy metals from wastewater by low-cost adsorbents. *J. Adv. Res.* **2011**, *2*, 297–303. [CrossRef]
3. Halawaa, R.A.E.; Zabin, S.A. Removal efficiency of Pb, Cd, Cu and Zn from polluted water using dithiocarbamate ligands. *J. Taibah Univ. Sci.* **2017**, *11*, 57–65. [CrossRef]
4. Zhong, L.S.; Hu, J.S.; Liang, H.P.; Cao, A.M.; Song, W.G.; Wan, L.J. Self-Assembled 3D Flowerlike Iron Oxide Nanostructures and Their Application in Water Treatment. *Adv. Mater.* **2006**, *18*, 2426–2431. [CrossRef]
5. Maiti, M.; Sarkar, M.; Malik, M.A.; Xu, S.; Li, Q.; Mandal, S. Iron Oxide NPs Facilitated a Smart Building Composite for HeavyMetal Removal and Dye Degradation. *ACS Omega* **2018**, *3*, 1081–1089. [CrossRef]
6. Gisi, S.D.; Lofrano, G.; Grassi, M.; Notarnicola, M. Characteristics and adsorption capacities of low-cost sorbents for wastewater treatment: A review. *Sustain. Mater. Technol.* **2016**, *9*, 10–40.
7. WHO. *Guidelines for Drinking Water Quality*; WHO: Geneva, Switzerland, 2017; Volume 4, pp. 327–398.
8. Shabani, K.S.; Ardejani, F.D.; Badii, K.; Olya, M.E. Preparation and characterization of novel nanomineral for the removal of several heavy metals from aqueous solution: Batch and continuous systems. *Arab. J. Chem.* **2017**, *10*, S3108–S3127. [CrossRef]
9. Jaishankar, M.; Tseten, T.; Anbalagan, N.; Mathew, B.B.; Beeregowda, K.N. Toxicity, mechanism and health effects of some heavy metals. *Interdiscip Toxicol.* **2014**, *7*, 60–72. [CrossRef]
10. Chodak, A.D.; Baszczyk, U. The Impact of Nickel on Human Health. *J. Elementol.* **2008**, *13*, 685–696.
11. Tchounwou, P.B.; Yedjou, C.G.; Patlolla, A.K.; Sutton, D.J. Heavy Metals Toxicity and the Environment. *EXS* **2012**, *101*, 133–164.
12. Lv, D.; Zheng, L.; Zhang, H.; Deng, Y. Mechanistic Insight into Disinfection Using Ferrate(VI). *Environ. Sci. Water Res. Technol.* **2018**, *4*, 701–710. [CrossRef]

13. Barakat, M.A. New trends in removing heavy metals from industrial wastewater. *Arab. J. Chem.* **2011**, *4*, 361–377. [CrossRef]
14. Karnib, M.; Kabbani, A.; Holail, H.; Olama, Z. Heavy Metals Removal Using Activated Carbon, Silica and Silica Activated Carbon Composite. *Energy Procedia* **2014**, *50*, 113–119. [CrossRef]
15. Dave, P.N.; Chopda, L.V. Application of Iron Oxide Nanomaterials for the Removal of Heavy Metals. *J. Nanotechnol.* **2014**, *2014*, 1–14. [CrossRef]
16. Lu, H.; Wang, J.; Stoller, M.; Wang, T.; Bao, Y.; Hao, H. An Overview of Nanomaterials for Water and Wastewater Treatment. *Adv. Mater. Sci. Eng.* **2016**, *2016*, 1–10. [CrossRef]
17. Amin, M.T.; Alazba, A.A.; Manzoor, U. A Review of Removal of Pollutants from Water/Wastewater Using Different Types of Nanomaterials. *Adv. Mater. Sci. Eng.* **2014**, *2014*, 1–24. [CrossRef]
18. Velez, E.; Campillo, G.E.; Morales, G.; Hincapie, C.; Osorio, J.; Arnache, O.; Uribe, J.I.; Jaramillo, F. Mercury removal in wastewater by iron oxide nanoparticles. *J. Phys. Conf. Ser.* **2016**, *687*, 1–4. [CrossRef]
19. Ismadji, S.; Soetaredjo, F.E.; Ayucitra, A. Natural Clay Minerals as EnvironmentalCleaning Agents. *Clay Mater. Environ. Remediat.* **2015**, *8*, 5–18.
20. Navaratne, A.; Priyantha, N.; Kulasooriya, T.P.K. Removal of Heavy Metal Ionsusing Rice Husk and Brick Clay as Adsorbents–Dynamic Conditions. *IJEE* **2013**, *6*, 807–814.
21. Bandara, C.; Priyantha, N. Chemical modification of thermally treated peat for removal of heavy metals in effluents. *Symp. Proc. Int. Symp. Water Qual. Hum. Health* **2012**, *4*, 52.
22. Agarwal, A.K.; Kadu, M.S.; Pandhurnekar, C.P.; Muthreja, I.L. Kinetics Study on the Adsorption of Ni^{2+} Ions onto Fly Ash. *J. Chem. Technol. Metall.* **2015**, *50*, 601–610.
23. Igwe, J.C.; Abia, A.A. Adsorption isotherm studies of Cd (II), Pb (II) and Zn (II) ions bioremediation from aqueous solution using unmodified and EDTA-modified maize cob. *Eclet. Quim.* **2007**, *32*, 33–42. [CrossRef]
24. Senevirathne, H.M.M.S.; Bandara, J.M.R.S. Cadmium and other heavy metal removal from contaminated drinking and irrigation water. *Symp. Proc. Int. Symp. Water Qual. Hum. Health* **2012**, *4*, 48.
25. Wijesinghe, W.P.S.L.; Mantilaka, M.M.M.G.P.G.; Peiris, T.A.N.; Rajapakse, R.M.G.; Wijayantha, K.G.U.; Pitawala, H.M.T.G.A.; Premachandra, T.N.; Herath, H.M.T.U.; Rajapakse, R.P.V.J. Preparation and characterization of mesoporous hydroxyapatite with non-cytotoxicity and heavy metal adsorption capacity. *New J. Chem.* **2018**, *42*, 10271–10278. [CrossRef]
26. Saeed, K.A.; Kassim, K.A.; Nur, H.; Yunus, N.Z.M. Strength of lime-cement stabilized tropical lateritic clay contaminated by heavy metals. *KSCE J. Civ. Eng.* **2014**, *19*, 887–892. [CrossRef]
27. Latifi, N.; Marto, A.; Eisazadeh, A. Structural Characteristics of Laterite Soil Treated by SH-85 and TX-85 (Non-Traditional) Stabilizers. *Electron. J. Geotech. Eng.* **2013**, *18*, 1707–1718.
28. Maignien, R. Review of research on laterites. *UNESCO* **1966**, *26-77*, 126–133.
29. Abdalla, M.A.; Jaafar, M.; Alothman, Z.A.; Alfadul, S.M. New Route for Preparation and Characterization of Magnetite Nanoparticles. *Arab. J. Chem.* **2010**, *4*, 235–237. [CrossRef]
30. Ghosh, M.K.; Pionern, E.; Issa, T.B.; Singh, P. Arsenic Adsorption on Goethite Nanoparticles Produced through Hydrazine sulfate Assisted Synthesis Method. *Korean J. Chem. Eng.* **2012**, *29*, 95–102. [CrossRef]
31. Sangami, S.; Manu, B. Synthesis of green iron nanoparticles using laterite and their application as a Fenton-like catalyst for the degradation of herbicide Ametryn in water. *Environ. Tech. Innov.* **2017**, *8*, 150–163. [CrossRef]
32. Dissanayake, D.M.S.N.; Mantilaka, M.M.M.G.P.G.; Palihawadana, T.C.; Chandrakumara, G.T.D.; De Silva, R.T.; Pitawala, H.M.T.G.A.; Nalin de Silva, K.M.; Amaratunga, G.A.J. Facile and low-cost synthesis of pure hematite (α-Fe_2O_3) nanoparticles from naturally occurring laterites and their superior adsorption capability towards acid-dyes. *RSC Adv.* **2019**, *9*, 21249–21257. [CrossRef]
33. Brasileiro, I.L.O.; Madeira, V.S.; de Souza, C.P.; Lopes-Moriyama, A.L.; Ramalho, M.L.R.A.; Araujo, A.D. Development of α-Fe_2O_3/Nb_2O_5 photocatalysts by a Pechini sol-gel route: Structural, morphological and optical influence. *Mater. Res. Express* **2019**, *6*, 015043. [CrossRef]
34. Dayananda, K.E.D.Y.T.; Gunawardhana, B.P.N.; Dissanayake, D.M.S.N.; Mantilaka, M.M.M.G.P.G.; Rajapakse, R.M.G.; Nalin de Silva, K.M.; Amaratunga, G.A.J.; Pitawala, H.M.T.G.A. Low Cost, Novel Synthesis Methods of Heamatite Nanoparticles from Sri Lankan Iron Rich Laterites. *Book Abstr. 4th ICNSNT* **2017**, *66*, 81.
35. Jayarathna, L.; Bandara, A.; Ng, W.J.; Weerasooriya, R. Fluoride adsorption on γ–Fe_2O_3 nanoparticles. *J. Environ. Health Sci. Eng.* **2015**, *13*, 54. [CrossRef]

36. Fu, F.; Wang, Q. Removal of heavy metal ions from wastewaters: A review. *J. Environ. Manag.* **2011**, *92*, 407–418. [CrossRef]
37. Grover, V.A.; Hu, J.; Engates, K.E.; Shipley, H.J. Adsortion and Desorption of Bivalent Metals to Hematite Nanoparticles. *Environ. Toxicol. Chem.* **2012**, *31*, 86–92. [CrossRef] [PubMed]
38. Dias, P.; Vilanova, A.; Lopes, T.; Andrade, L.; Mendes, A. Extremely stable bare heamatite photoanode for solar water splitting. *Nano Energy* **2016**, *23*, 70–79. [CrossRef]
39. Sivula, K.; Zboril, R.; Formal, F.L.; Robert, R.; Weidenkaff, A.; Tucek, J.; Frydrych, J.; Gratzel, M. Photoelectrochemical Water Splitting with Mesoporous Heamatite Prepared by a Solution-Based Colloidal Approach. *J. Am. Chem. Soc.* **2010**, *132*, 7436–7452. [CrossRef]
40. Lassoued, A.; Lassoued, M.S.; Dkhil, B.; Ammar, S.; Gadri, A. Photocatalytic degradation of methylene blue dye by iron oxide (α-Fe_2O_3) nanoparticles under visible irradiation. *J. Mater. Sci.Mater. Electron.* **2018**, *10*, 1007–1012. [CrossRef]
41. Chirita, M.; Grozescu, I. Fe_2O_3–Nanoparticles, Physical Properties and Their Photochemical And Photoelectrochemical Applications. *Chem. Bull. POLITEHNICA* **2009**, *54*, 68–72.
42. Basavegowda, N.; Mishra, K.; Lee, Y.R. Synthesis, characterization, and catalytic applications of heamatite (α-Fe_2O_3) nanoparticles as reusable nanocatalyst. *Adv. Nat. Sci: Nanosci. Nanotechnol.* **2017**, *8*, 1–6.
43. Yadav, A.A.; Deshmukh, T.B.; Deshmukh, R.V.; Patil, D.D.; Chavan, U.J. Electrochemical super capacitive performance of Heamatite α-Fe_2O_3 thin films prepared by spray pyrolysis from non-aqueous medium. *Thin Solid Film.* **2016**, *616*, 351–358. [CrossRef]
44. Zhu, W.; Cui, X.; Liu, X.; Zhang, L.; Huang, J.Q.; Piao, X.; Zhang, Q. Hydrothermal evolution, optical and electrochemical properties of hierarchical porous heamatite nanoarchitectures. *Nanoscale Res. Lett.* **2013**, *8*, 1556–1570. [CrossRef] [PubMed]
45. Wanga, F.; Lu, X.; Li, X.Y. Selective removals of heavy metals (Pb^{2+}, Cu^{2+} and Cd^{2+}) from wastewater by gelation with alginate for effective metal recovery. *J. Hazard. Mater.* **2016**, *308*, 75–83. [CrossRef] [PubMed]
46. Fernando, M.S.; de Silva, R.M.; de Silva, K.M.N. Synthesis, characterization, and application of nano hydroxyapatite and nanocomposite of hydroxyapatite with granular actvated carbon for the removal of Pb^{2+} from aqueous solutions. *J. App. Surf. Sci.* **2015**, *351*, 95–103. [CrossRef]
47. Sahoo, S.K.; Agarwal, K.; Singh, A.K.; Polke, B.G.; Raha, K.C. Characterization of γ- and α-Fe_2O_3 nano powders synthesized by emulsion precipitation-calcination route and rheological behaviour of α-Fe_2O_3. *IJEST* **2010**, *2*, 118–126.
48. Lassoued, A.; Dkhil, B.; Gadri, A.; Ammar, S. Control of the shape and size of iron oxide (α-Fe_2O_3) nanoparticles synthesized through the chemical precipitation method. *Results Phys.* **2017**, *7*, 3007–3015. [CrossRef]
49. Rajapaksha, A.U.; Vithanage, M.; Weerasooriya, R.; Dissanayake, C.B. Surface complexation of nickel on iron and aluminum oxides: A comparative study with single and dual site clays. *Colloids Surf. A.* **2012**, *405*, 79–88. [CrossRef]
50. Shrestha, S. Modeling of Experimental Adsorption Isotherm Data. *J. Chem. Eng. Process Technol.* **2016**, *7*, 295–302.
51. Qian, H.; Han, G.; Yang, H.; Lin, G.; Xu, R. Investigation on Magnetic Properties of Heamtite Superstructures with Controlled Microstructures. *ASEAN J. Chem. Eng.* **2008**, *8*, 51–60.
52. Lin, M.; Tng, L.; Lim, T.; Choo, M.; Zhang, J.; Tan, H.R.; Bai, S. Hydrothermal Synthesis of Octadecahedral Hematite (α-Fe_2O_3) Nanoparticles: An Epitaxial Growth from Goethite (α-FeOOH). *J. Phys. Chem. C* **2014**, *118*, 10903–10910. [CrossRef]
53. Macera, L.; Taglieri, G.; Daniele, V.; Passacantando, M.; D'Orazio, F. Nano-sized Fe(III) oxide particles starting from an innovative and eco-friendly synthesis method. *Nanomaterials* **2020**, *10*, 323. [CrossRef] [PubMed]
54. Kruk, M.; Jaroniec, M.; Sayari, A. Application of Large Pore MCM-41 Molecular sieves to improve pore size analysis using nitrogen adsorption measurements. *Langmuir* **1997**, *13*, 6267–6273. [CrossRef]
55. Fard, A.K.; Rhadfi, T.; Mckay, G.; Al-marri, M.; Abdala, A.; Hilal, N.; Hussien, M.A. Enhancing oil removal from water using ferric oxide nanoparticles doped carbon nanotubes adsorbents. *Chem. Eng. J.* **2016**, *293*, 90–133. [CrossRef]
56. Kadirvelu, K.; Kavipriya, M.; Karthika, C.; Radhika, M.; Vennilamani, N.; Pattabhi, S. Utilization of Various Agricultural Wastes for Activated Carbon Preparation and Application for the Removal of Dyes and Metal Ions from Aqueous Solutions. *Bioresour. Technol.* **2003**, *87*, 129–132. [CrossRef]

57. Tan, W.T.; Ooi, S.T.; Lee, C.K. Removal of chromium(VI) from solution by coconut husk and palm pressed fibres. *Environ. Technol.* **1993**, *14*, 277–282. [CrossRef]
58. Gunathilake, C.; Kadanapitiye, M.S.; Dudarko, O.; Huang, S.D.; Jaroniec, M. Adsorption of Lead ions from Aqeous Phase on Mesoporous Silica with P-Containing Pendant Groups. *ACS Appl. Mater. Interfaces* **2015**, *7*, 23144–23152. [CrossRef]
59. Jacob, J.M.; Karthik, C.; Saratale, R.G.; Kumar, S.S.; Prabakar, D.; Kadirvelu, K.; Pugazhendhi, A. Biological approaches to tackle heavy metal pollution: A survey of literature. *J. Environ. Manag.* **2018**, *217*, 56–70. [CrossRef]
60. Anirudhan, T.S.; Sreekumari, S.S. Adsorptive removal of heavy metal ions from industrial effluents using activated carbon derived from waste coconut buttons. *J. Environ. Sci.* **2011**, *23*, 1989–1998. [CrossRef]
61. Asuquo, E.D.; Martin, A.D.; Nzerem, P. Evaluation of Cd(II) Ion Removal from Aqeous Solution by a Low-Cost Adsorbent Prepared from White Yam (Dioscorea rotundata) Waste using Batch Sorption. *ChemEngineering* **2018**, *2*, 35. [CrossRef]
62. Osinska, M. Removal of lead(II), copper(II), cobalt(II) and nickel(II) ions from aqeous solutions using carbon gels. *J. Sol Gel Sci. Technol.* **2017**, *81*, 678–692. [CrossRef]
63. Li, Y.H.; Ding, J.; Luan, Z.; Wang, S. Adsorption of Cadmium (II) From Aqeous Solution by Surface Oxidized Carbon Nanotubes. *Carbon* **2003**, *41*, 1057–1062. [CrossRef]
64. Kaur, R.; Vatta, P.; Kaur, M. Carbon Nanotubes: A Review Article. *IJRASET* **2018**, *6*, 5075–5079. [CrossRef]